Journal of Applied Geophysics 119 (2015) 178–191

Contents lists available at ScienceDirect

Journal of Applied Geophysics

journal homepage: www.elsevier.com/locate/jappgeo

Combining airborne electromagnetic and geotechnical data for automated depth to bedrock tracking

Craig William Christensen [a,b,1], Andreas Aspmo Pfaffhuber [a,*], Helgard Anschütz [a], Tone Fallan Smaavik [a]

[a] Norwegian Geotechnical Institute, 72 Sognsveien, Postboks 3930, 0806 Oslo, Norway
[b] Queen's University, Department of Geosciences and Geological Engineering, Bruce Wing/Miller Hall, 36 Union Street, Kingston, Ontario, K7L 3N6, Canada

ARTICLE INFO

Article history:
Received 31 October 2014
Received in revised form 30 April 2015
Accepted 3 May 2015
Available online 12 May 2015

Keywords:
Engineering geophysics
Geotechnical investigation
Airborne electromagnetic
Depth to bedrock
Interpolation
Geostatistical modeling

ABSTRACT

Airborne electromagnetic (AEM) survey data was used to supplement geotechnical investigations for a highway construction project in Norway. Heterogeneous geology throughout the survey and consequent variable bedrock threshold resistivity hindered efforts to directly track depth to bedrock, motivating us to develop an automated algorithm to extract depth to bedrock by combining both boreholes and AEM data. We developed two variations of this algorithm: one using simple Gaussian or inverse distance weighting interpolators, and another using ordinary kriging and combined probability distribution functions of input parameters.

Evaluation shows that for preliminary surveys, significant savings in boreholes required can be made without sacrificing bedrock model accuracy. In the case study presented, we estimate data collection savings of 1000 to 10,000 NOK/km (c. $160 to $1600 USD/km) would have been possible for early phases of the investigation. However, issues with anthropogenic noise, low signal, and uncertainties in the inversion model likely reduced the comparative advantage that including AEM provided.

AEM cannot supersede direct sampling where the model accuracy required exceed the resolution possible with the geophysical measurements. Nevertheless, with the algorithm we can identify high probability zones for shallow bedrock, identify steep or anomalous bedrock topography, and estimate the spatial variability of depth at earlier phases of investigation. Thus, we assert that our method is still useful where detailed mapping is the goal because it allows for more efficient planning of secondary phases of drilling.

1. Introduction

Using geophysical methods in geotechnical site investigations for transport corridors is common practice. Compared to direct sampling methods (i.e. drilling, excavation), subsurface data can be acquired with much fuller coverage at a much lower cost. However, to date, such techniques have been generally limited to localized surveys using ground-based techniques. This includes seismic methods (Michaels, 1999, 2004; Rucker, 2000), ground penetrating radar (Nichol and Reynolds, 1999), and geoelectric methods including electrical resistivity tomography (ERT) and electromagnetics (EM) (Ngan-Tillard et al., 2010; Sauvin et al., 2013; Solberg et al., 2012). While the use of airborne systems is apparently rare for surface transport projects, Pfaffhuber et al. (2010) and Okazaki et al. (2011) document recent examples where airborne electromagnetic (AEM) surveys were used for tunnel pre-investigations.

Regardless of the scale of the geophysical survey, the cost-saving potential of the technique is impeded by difficulties in interpretation. Geophysical properties of a lithological unit may show regional trends, yet they are site-specific and may be locally heterogeneous (Beamish, 2013), meaning extracting a useful final product is not straightforward. The traditional approach is knowledge-based (cognitive) modeling, where practitioners manually take into account multiple data sources such as boreholes, surface observations, and geophysical surveys to construct a model. Recent examples such as Foged (2014) and Jørgensen et al. (2013) show that this approach can still be useful because they produce more nuanced models than more automated methods; however, they are subjective, difficult to repeat, and time-consuming to produce. Constrained inversion is more repeatable and objective, but limited to cases with very simple geology and a narrow scope of required engineering parameters (Chouteau et al., 2013; Foged et al., 2014). In more complex geological settings, combining unconstrained inversion results with other data sets using geostatistical techniques to determine appropriate cutoff values is often more appropriate, as demonstrated by studies in sedimentary settings such as He et al.

* Corresponding author.
E-mail addresses: craig.christensen@ucalgary.ca (C.W. Christensen), AAP@ngi.no (A.A. Pfaffhuber), HAn@ngi.no (H. Anschütz), TFS@ngi.no (T.F. Smaavik).
[1] Present address: University of Calgary, Department of Geoscience, 844 Campus Place Northwest, Calgary, Alberta T2N 1 N4, Canada.

http://dx.doi.org/10.1016/j.jappgeo.2015.05.008

(2014), and Strebelle (2002). Also using artificial neural networks has proven useful for such settings (Gunnink et al., 2012).

Our study was motivated by one such example in engineering geophysics where extracting a useful quantitative model proved challenging. A 30 km section of the E16 highway northeast of Oslo, Norway is scheduled for reconstruction (Fig. 1). An AEM survey was used to, among other aims, map depth to bedrock and to fill in data gaps between drilling locations. While the resulting resistivity model and borehole logs showed similar trends, the resistivity at known bedrock locations varied between 60 and 2000 Ωm for reasons discussed in Section 2 (Field Data). Using a single-valued resistivity threshold produced a model that only partially matched ground truth data. Similarly, the time-consuming cognitive approach of manually creating a surface that matched both borehole depths and trends in the resistivity model also gave a model with unknown uncertainty. An example cross-section showing these early modeling efforts is shown in Fig. 2. In order for AEM surveys to successfully reduce the number of boreholes and excavations needed for geotechnical site investigations, we required an interpretation method that gave us more reliable model results.

This paper presents a new bedrock depth tracking algorithm to address this problem. By combining AEM inversion models and borehole data, this method should:

1. Account for variable bedrock threshold resistivity;
2. Quantify the uncertainty of prediction; and
3. Limit manual input from user (i.e. be automated).

By cross-validating the method using subsets of borehole data, we evaluate the potential cost savings in site-investigations of this type using AEM.

2. Field data

Our intention with this article is to describe and discuss the integration of AEM and geotechnical data rather than a detailed description of the survey details or results. We thus only briefly introduce the project, survey and processing and inversion details. A more detailed treatment of these can be found in Anschütz et al. (2014).

The section of road surveyed spans an area with primarily glacial sediments underlain by Precambrian bedrock. Deglaciation last occurred 9000– 10,000 years ago, and various glaciomarine, glaciofluvial, and modern fluvial deposits have since formed (Andersen, 1979; Norwegian Geological Survey, 2014; Ramberg et al., 2008). A map of surficial sediments is provided in Fig. 3. Based on borehole logs, glaciomarine clay is the dominant material, with some layers of silt. In large areas the clay is sensitive or quick through the entire overburden thickness. The bedrock here is part of the Gothian Orogenic belt referred to either the Romerike District or Åmål-Horred belt (Ramberg et al., 2008; Starmer, 1996). The region is dominated by a variety of supracrustal granitoid rocks, ranging from biotite-rich gneisses and mica schist, with amphibolite and hornblende gneiss appearing to a lesser degree (Ramberg et al., 2008). Despite having a somewhat heterogeneous composition (being a layered gneiss), these are all grouped into a single unit on the geological map (Norwegian Geological Survey

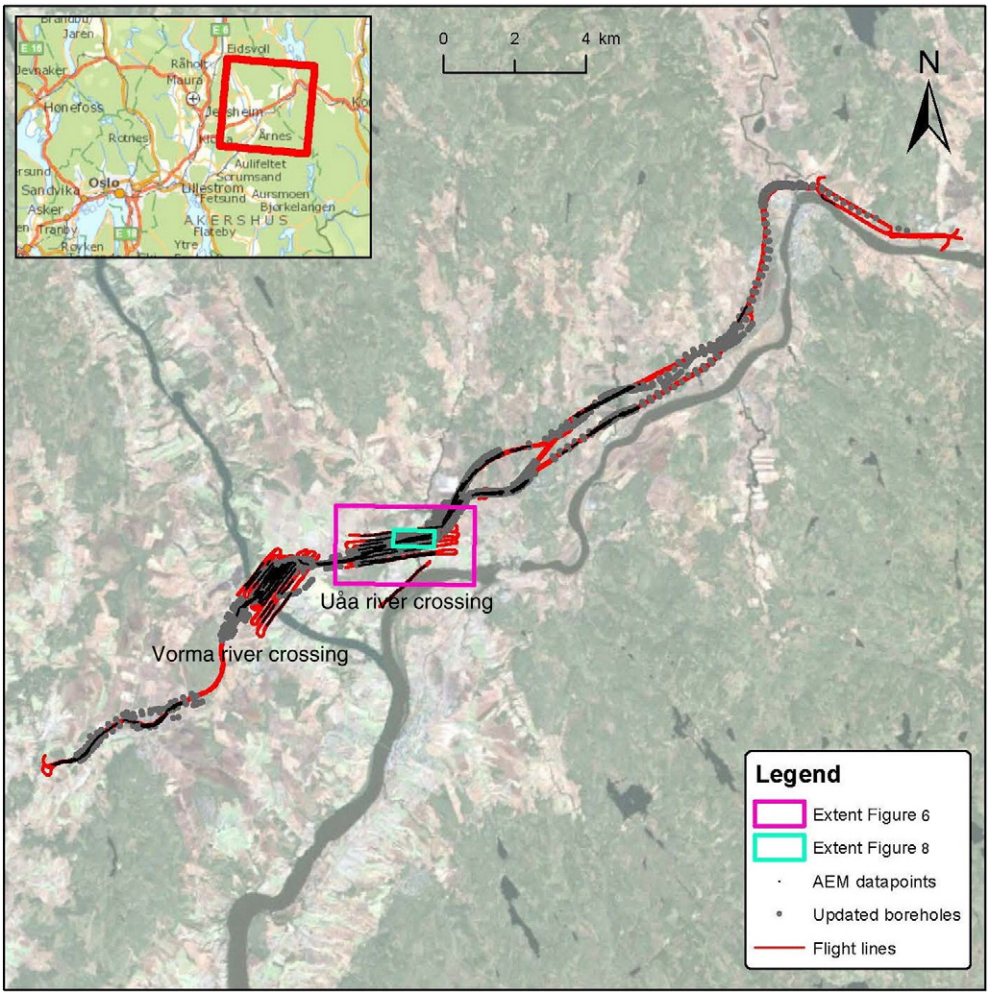

Fig. 1. Location maps for data collected for the E16 highway upgrade site investigation, with inset map showing location relative to Oslo, Norway.

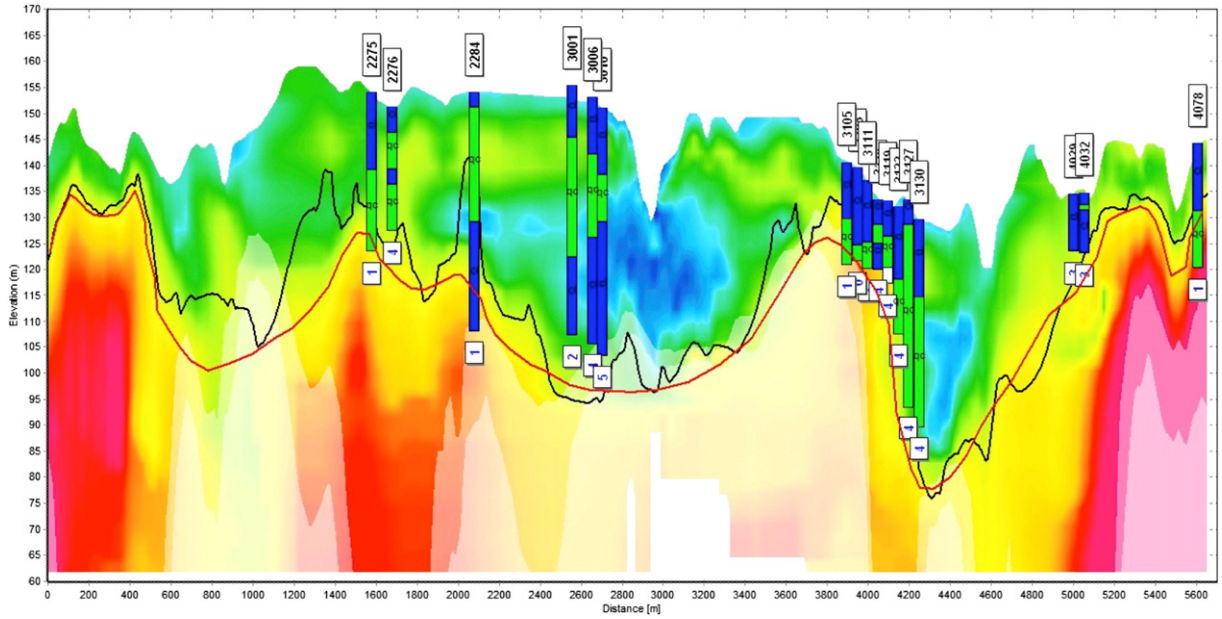

Fig. 2. An example profile located between the rivers Vorma and Uåa showing AEM-derived resistivity and boreholes (see Fig. 3 for color scale). Boreholes are marked by their identification numbers (4 digits) and their lateral distance to the AEM profile in [m] (1 digit). The red line depicts a manually picked bedrock layer, while the black line is an automatically picked 100 Ωm threshold (Figure from Anschütz et al., 2014).

www.ngu.no). Furthermore, there are no major geological contacts intersected by the survey. The closest is a major shear zone between the Romerike District and the older Trans-Scandinavian Igneous Belt (TSIB) which is 6 km northwest of the zone with overlapping AEM and borehole data (Ramberg et al., 2008; Starmer, 1996). Hence, while local variations in resistivity due to gneissic layering are expected, no sharp regional-scale boundaries in bedrock resistivity should be present.

While there are variations within overburden and bedrock material, conditions are nevertheless conducive to bedrock mapping with AEM. The area was presumably scoured bare by glaciation and most

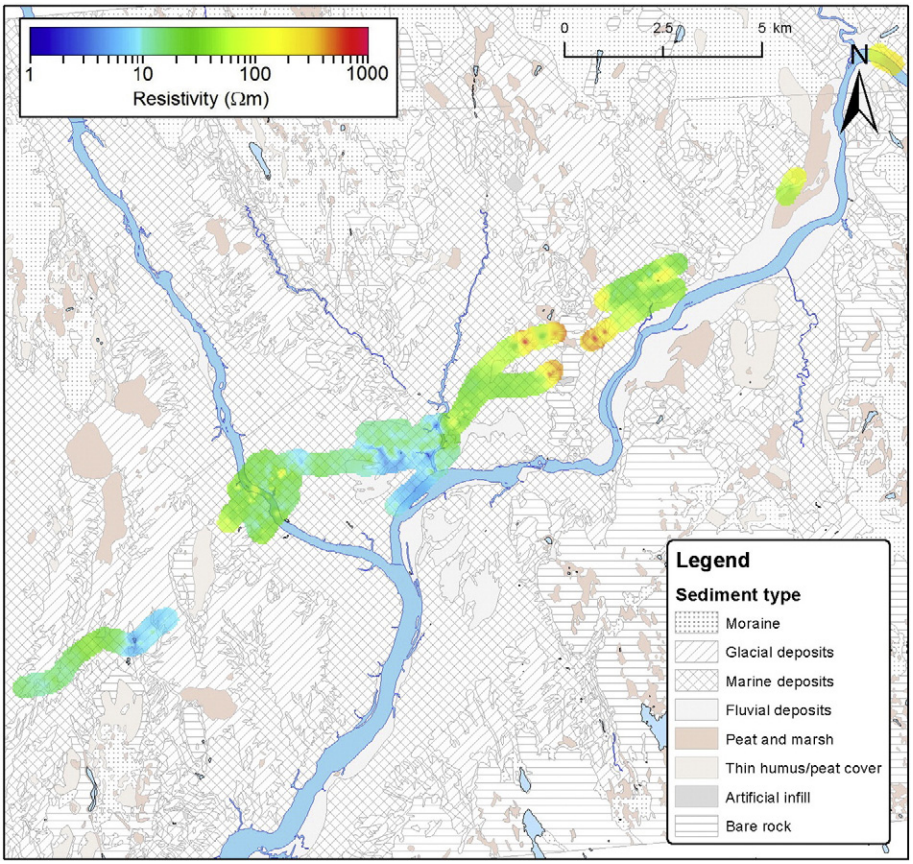

Fig. 3. Map of the average resistivity of the uppermost 5 m of the subsurface superimposed on surface sediment map retrieved from the Norwegian Geological Survey (2014).

sediments are allochthonous rather than in-situ. Therefore, the geometry of the contact between bedrock and overburden should presumably be quite sharp. Second, the magntiude of resistivity difference between bedrock and overburden is sufficiently large. Norwegian glaciomarine clays generally range from 1 to 100 Ωm (Rømoen et al., 2010; Solberg et al., 2012), and though no previous EM or resistivity measurements in this project area were encountered, Palacky (1987) states that nearly all unweathered metamorphic and igneous rocks have resistivities between 1000 and 100,000 Ωm. Hence, given the sharp geological contact and large difference in resistivities that are likely to occur in the area, the bedrock depth should be well-defined in our resistivity model despite variations in what resistivity value that transition occurs at.

The AEM survey was conducted with the SkyTEM 302 system using a 314 m^2 frame with two turns in the high moment and one turn in the low moment to obtain high near surface resolution. A general description of the system can be found in Sørensen and Auken (2004). A total of 178 line-km was flown in three consecutive days in January 2013. Three parallel lines with a spacing of 25 m were flown along the planned road corridor. Additional lines with nominal spacing 125 m covered two river crossings: 15 lines near Vorma/Vormsund, and 9 lines near Uåa (Fig. 1). Raw data were processed using the Århus workbench (www.aarhusgeo.com). Significant portions of the raw data were rejected for several reasons, either due to anthropogenic noise (primarily electrical transmission lines) or due to low signal from shallow or very resistive bedrock. Both layered and borehole-constrained inversions were attempted, but produced unsatisfactory results. This judgment was based on high residual values, poor fit with data, poor match with borehole measurements, and unrealistic configurations given what is known about the geological environment. Instead, using a smooth, a 1-D stitched spatially constrained inversion (sometimes called a "pseudo-3D" inversion) (Viezzoli et al., 2008) with fixed layer depth produced the best results. The final model used has 20 layers of logarithmically increasing thicknesses, ranging from 1.5 to 12.4 m. While the smoothed model better accounted for the complex geometry of overburden sediments, the smoothing may also contribute to the apparent variation in the bedrock threshold resistivity. Even in this model, however, the inversion method had difficulty converging on a resistivity value in many locations, leaving approximately 35% of AEM soundings with an undetermined uncertainty value.

At the time of this study, 1388 borehole locations were available, 842 of which were within 125 m from one AEM sounding. Over 92% of these were rotary pressure soundings, but total soundings were dug as well. These holes have a nominal spacing of 50 m along the proposed road alignment and at the bridge crossing at Vorma, while they are 100 m or more apart everywhere else. There is some uncertainty in the depth to bedrock measurements from rotary pressure soundings because

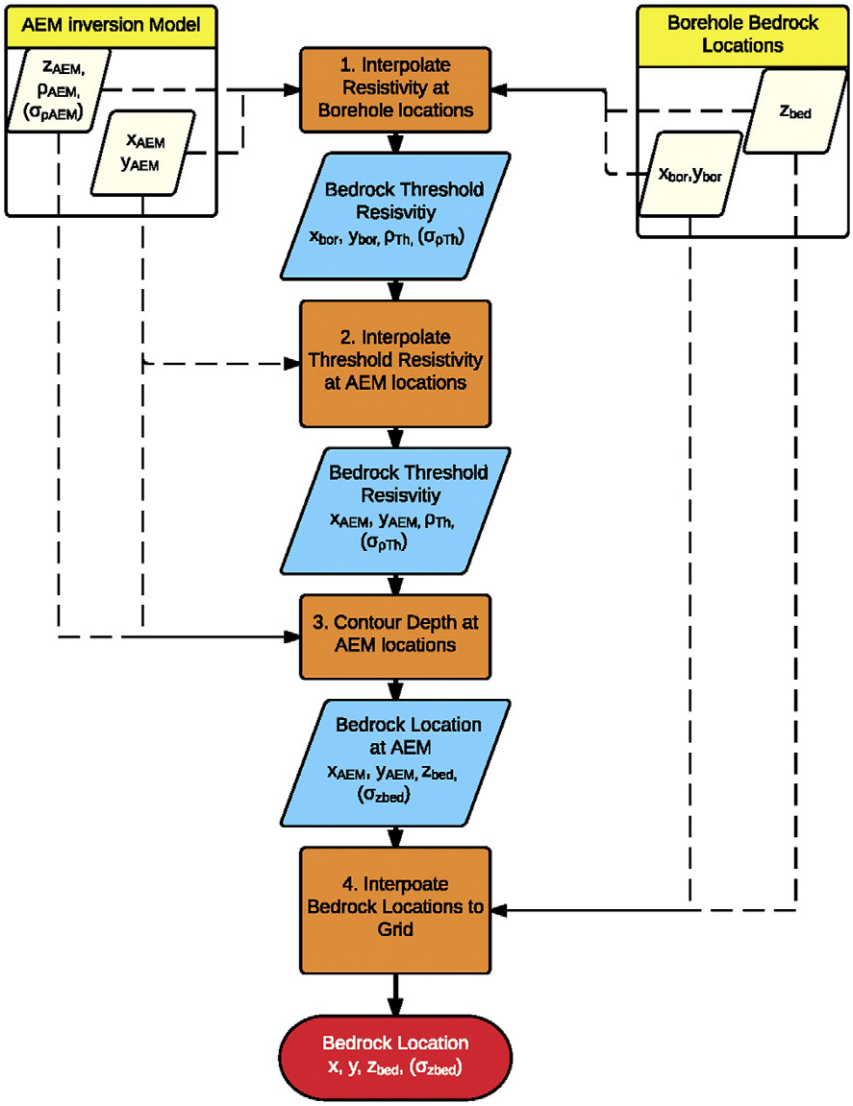

Fig. 4. Overview of data flow and major computational steps performed by the algorithm.

densely packed gravel or glacial erratics can give a similar response as bedrock.

3. Method

Fig. 4 outlines the main computation steps of the algorithm developed. The process uses two sets of data: vertical resistivity profiles at one set of x–y coordinates (AEM soundings), and depth to bedrock measurements at another set of x–y coordinates (boreholes). Step 1 finds an appropriate bedrock threshold resistivity for the bedrock surface by interpolating resistivity at the measured bedrock locations. Step 2 then interpolates the chosen bedrock threshold resistivities from bedrock locations onto the AEM sounding coordinates. In Step 3, depth to bedrock is chosen at the AEM locations based on the vertical resistivity profile, threshold resistivity, and an initial guess of the depth based on nearby boreholes. Finally, depth to bedrock is interpolated on a regular grid using both borehole measurements and predictions at AEM locations in Step 4.

Two different variations of the method were developed. These both varied the interpolator used in Steps 1, 2, and 4, and the depth selection process in Step 3. Variation 1, the simpler of the two, uses weighted arithmetic means based on distance from data points:

$$\bar{x} = \frac{\sum_{i=1}^{n} x_i \cdot w(r_i)}{\sum_{i=1}^{n} w(r_i)} \tag{1}$$

where:

$\bar{x}$	interpolated parameter value
n	number of input data values
x_i	i^{th} data value
w	weight function
r_i	distance to i^{th} data value

Two weighting functions were tested: inverse distance weighting (IDW) and Gaussian function

$$w_{IDW}(r) = \frac{1}{r^p} \tag{2}$$

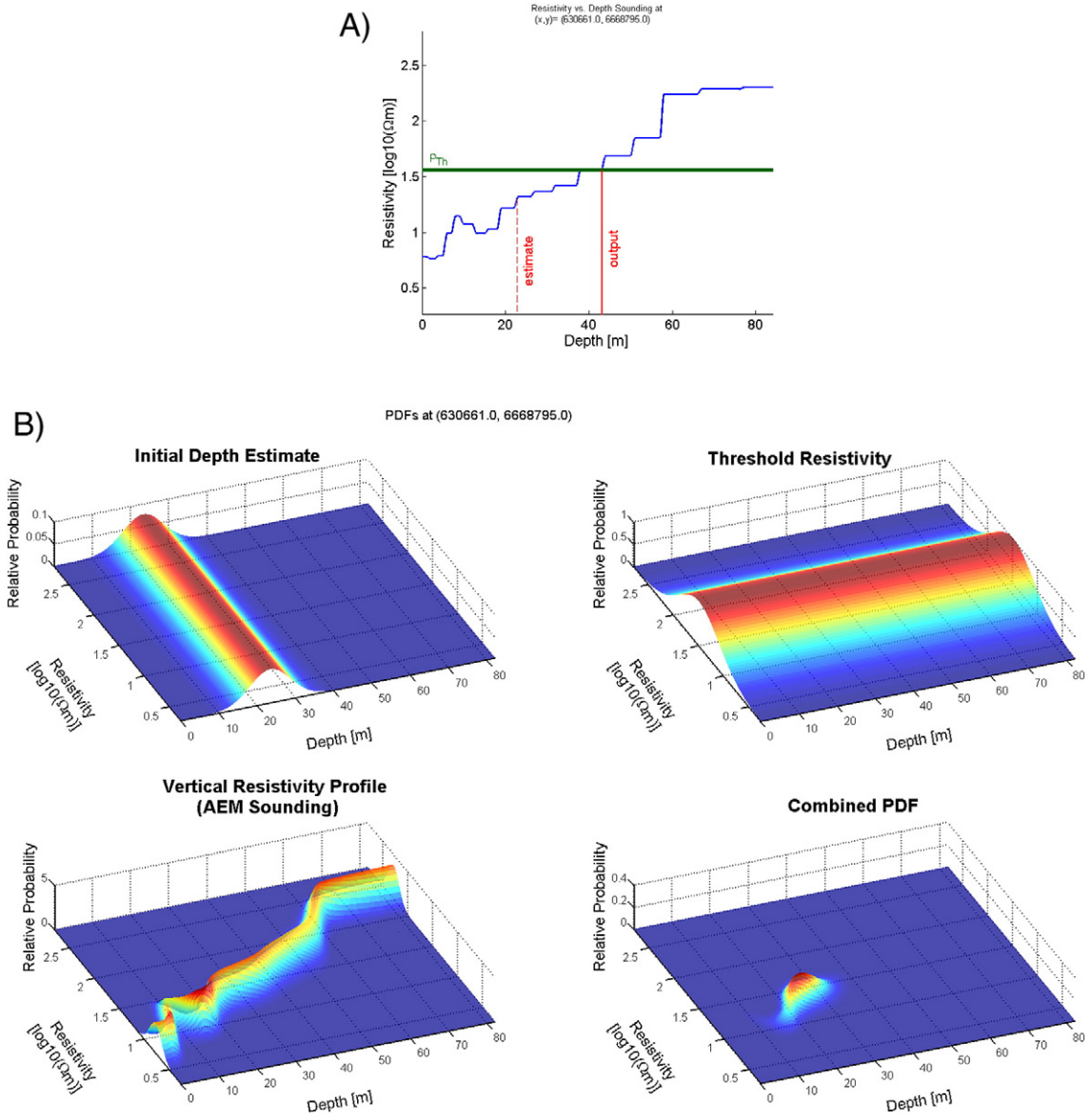

Fig. 5. Comparison of the depth to bedrock selection methods employed in Step 3. A) Variation 1 uses simple intersection of the vertical resistivity profile and threshold resistivity. B) Variation 2 employs multiple probability distribution functions.

Table 1
Comparison of the distribution of bedrock threshold resistivities between Variations and between the first two steps of the computation.

		Minimum [Ωm]	Median [Ωm]	Maximum [Ωm]
Step 1: bedrock threshold resistivities at boreholes	Variation 1	55	4.3×10^2	2.4×10^3
	Variation 2	31	4.6×10^2	2.0×10^3
Step 2: bedrock threshold resistivities at AEM soundings	Variation 1	55	3.8×10^2	1.6×10^3
	Variation 2	85	3.7×10^2	1.6×10^3

$$w_{Gaus}(r) = e^{-\frac{r^2}{2\sigma}} \quad (3)$$

where:

p IDW exponent
σ correlation distance parameter

In the case of 3D interpolation in Step 1, transverse anisotropy was modeled by specifying different horizontal and vertical relationships:

$$w_{IDW}(r_{xy}, r_z) = \frac{\alpha}{r_{xy}^p} + \frac{1}{r_z^p} \quad (4)$$

$$w_{Gaus}(r_{xy}, r_z) = e^{-\frac{r_{xy}^2}{2\sigma_{xy}} - \frac{r_z^2}{2\sigma_z}} \quad (5)$$

where:

r_{xy}, r_z horizontal and vertical distance
α ratio of horizontal to vertical distance weighting
σ_{xy}, σ_z horizontal and vertical correlation parameters

To select depth at AEM soundings in Step 3, Variation 1 simply finds the depth at which the vertical resistivity profile and threshold resistivity intersect (Fig. 5A). In the case where there is more than one intersection, the intersection closest to the initial depth estimate becomes the prediction used.

In Variation 2, more advanced geostatistical methods are applied. Kriging is used to interpolate in steps 1, 2, 4. While more computationally demanding, kriging has several advantages: it uses a data-derived rather than arbitrary interpolation function; it optimized interpolation weights based on data configuration; and offers a way to calculate uncertainty of the predicted value. For each kriging interpolation, two separate kriging calculations are performed: one for the model parameter, and one for the uncertainty of the parameter. An experimental semi-variogram is calculated for both, and a theoretical semi-variogram modeled using a least-squares fitting routine developed by Schwanghart (2010). Model parameter and model parameter errors are interpolated, and the kriging variance of the model parameter is also calculated. Total uncertainty of the model parameter then becomes (Pryet et al., 2011):

$$\sigma_{tot}^2 = \sigma_{krig}^2 + \sigma_{err}^2 \quad (6)$$

where:

σ_{tot}^2 total parameter variance
σ_{krig}^2 kriging variance
σ_{err}^2 variance due to model parameter error

Parameter variances are thus carried through by using total variance of a model parameter in one step as the input error parameter in the next interpolation step.

In all cases, ordinary kriging in two dimensions using an isotropic variogram model is the form of kriging used. Due of the long, linear configuration of the data, automatically fitting an anisotropic variogram becomes difficult. There are relatively few pairs of data aligned perpendicular to the orientation of the planned road, meaning a reasonable variogram model cannot be fit for all directions. Furthermore, for Step 1 specifically, the assumption of data stationarity, an important

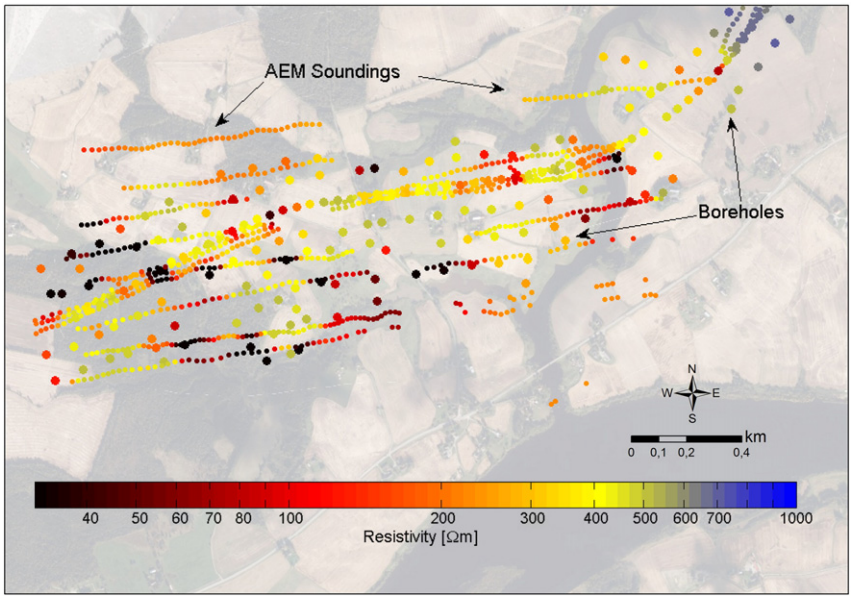

Fig. 6. An illustration of the variability in bedrock threshold resistivity calculated near Uåa by the tracking algorithm (Variation 1, Steps 1 & 2).

condition for kriging, does not fit well because of the strong vertical trend in resistivity. Given that the resistivity model used has depth layers with consistent thickness, the method employed by Pryet et al. (2011), wherein resistivity was kriged in 2D in each model layer separately, was adopted.

Additionally, rather than using a simple intersect, Variation 2 selects depth to bedrock in Step 3 using multiple Probability Distribution Functions (PDFs). At each AEM sounding, three two-dimensional PDFs are modeled on the resistivity-depth plane, one each for the initial depth estimate (Fig. 5Bi), the bedrock threshold resistivity (Fig. 5Bii), and the vertical resistivity profile (Fig. 5Biii). These are multiplied together to produce a combined PDF (Fig. 5Biv). This surface is integrated over small strips parallel to the resistivity axis to produce a one-dimensional probability versus depth curve. A normal distribution is then fit to this curve, and the mean and standard deviation are returned as the depth to bedrock and depth uncertainty.

Finally, we made two important choices in data handling applicable to both variations. First of all, resistivity data was transformed using a base-10 logarithm before any calculation. Given that resistivity values are distributed over several orders of magnitude, the interpolated values would have been strongly skewed by large values without the transformation. Furthermore, kriging provides the best linear unbiased estimator when data are close to normally distributed, and resistivity data is often lognormally distributed (Chilès and Delfiner, 2011). Second, all interpolation in Step 1 was performed in x–y-depth space rather than x–y–z space. Initial runs showed that x–y–z interpolation of resistivity produced a staircase-like model where layer thicknesses changed abruptly at midpoints between AEM soundings. Doing x–y-depth interpolation instead allowed layer thicknesses to vary more continuously, which was assumed to be a more realistic treatment.

After running each Variation on the full data set, the performance of the algorithm was evaluated using cross validation. We input a random number and combination of boreholes plus all of the AEM data. Then, we used the algorithm to predict the depth to bedrock at borehole locations that were not given to the interpolator, and compared the predictions to the measure depth values. We repeated this for the same subset of boreholes, but excluded the AEM data. 1500 trials were performed for Variation 1, and 500 were performed for Variation 2. Additionally, for Variation 2, standard scores of depth predictions were calculated

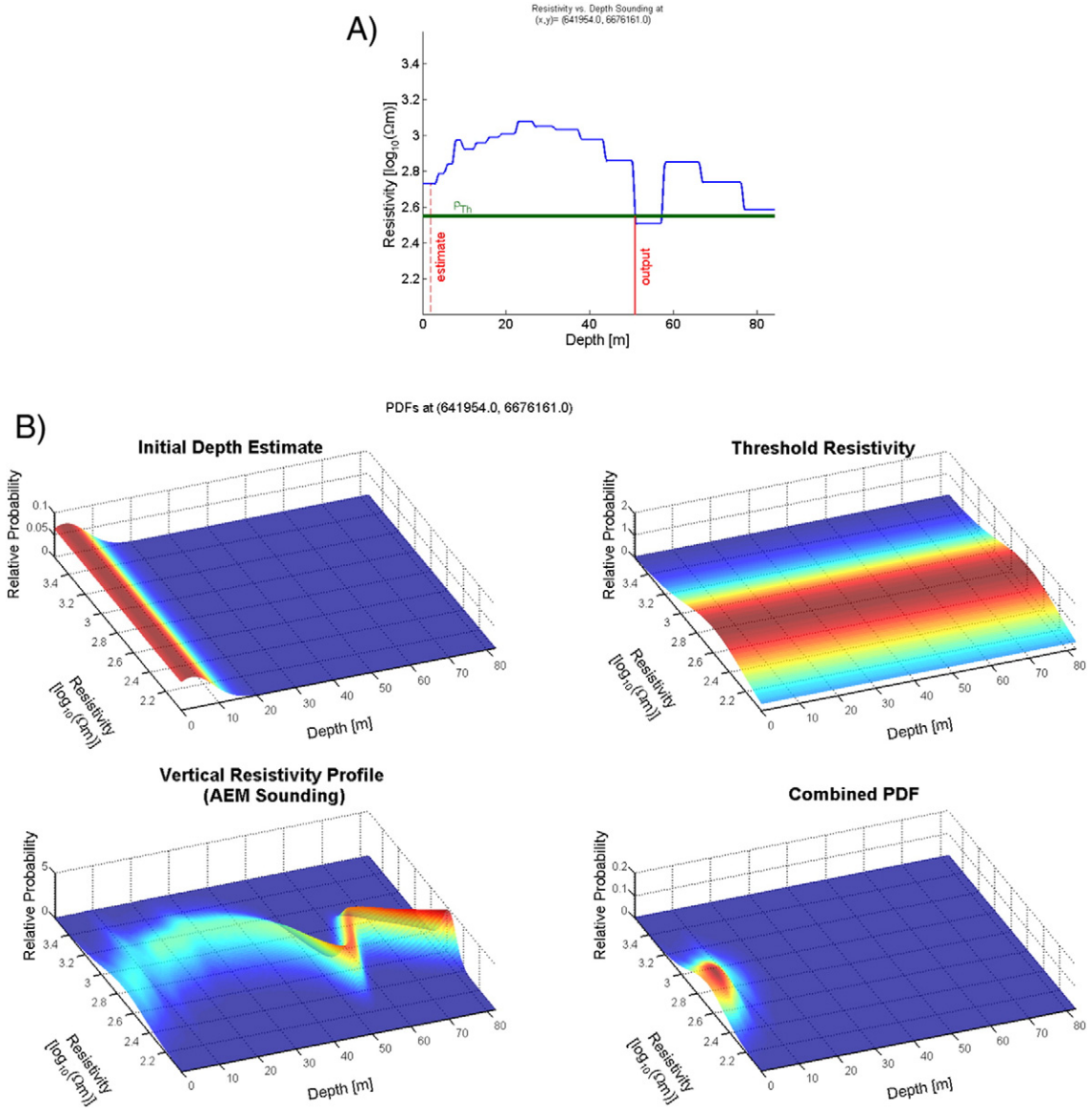

Fig. 7. A) While the method used by Variation 1 to selected depth to Bedrock in Step 3 usually suffices, it fails where there are large uncertainties in input parameters. B) Variation 2's method provides a more reliable choice in depth because these uncertainties are considered.

based on the calculated prediction uncertainty and the measured depth values:

$$Z = \frac{d_p - d_{obs}}{\sigma_d} \tag{7}$$

where:

Z	standard score of depth prediction
d_p	depth prediction
d_{obs}	measured (observed) depth
σ_d	estimated uncertainty of depth prediction

4. Results

When using the full set of AEM and borehole data, results from intermediary steps of either Variation show similar trends. The difference are not very large in Steps 1 and 2. Despite the dissimilar interpolation functions, the distribution of threshold resistivities selected are similar (Table 1), and have a high degree of spatial variability (Fig. 6). In Step 3, the simple intersection method used by Variation 1 gives nearly the same depth selection as the PDF method used by Variation 2. However, Variation 1 rejects at least 5% of depth selections because they are more than 20 m from the original estimate. As Fig. 7 shows, Variation 2 has a performance edge in such difficult to interpret cases.

The final depth to bedrock grids diverge significantly, however. Fig. 8 shows a zoomed in samples of the algorithms output. Both Variation 1 and 2 show that adding AEM data gives enhanced detail to the bedrock map, compared to borehole information only. However, Variation 1 does not successfully find depth to bedrock at many AEM soundings, which limits the coverage of the resulting map. Additionally, Variation 1 does not give an estimate of uncertainty, while the map from Variation 2 clearly shows the limits of certainty and how AEM reduces uncertainty (which is represented by the fading white overlay). Furthermore, the depths selected at a large distance from the boreholes vary substantially, by up to 40 m in some cases.

Despite the differing results, both Variations face two similar obstacles. First of all, while the entire calculation is automated, some time was needed to select appropriate interpolation parameters. Second, between 35% and 40% of all AEM soundings lacked a valid depth selection after Step 3. Most of these are locations where, as described in Section 2 (Field Data), raw data was rejected due to noise or low signal, or where the inverted resistivity model had too large of an uncertainty. Some of these were also due to the limitations of the contouring algorithm. Variation 1 requires an exact match between bedrock threshold resistivity and the vertical resistivity profile to find depth in Step 3, but in areas of shallow bedrock, the resistivity does not have sufficient resolution to capture this transition from sediment to bedrock. This was often the case in the northeastern portion of the survey area, where bedrock was nearly at surface and sometimes outcropping. As well, depth picks which deviated more than 20 m from the initial guess based on nearly

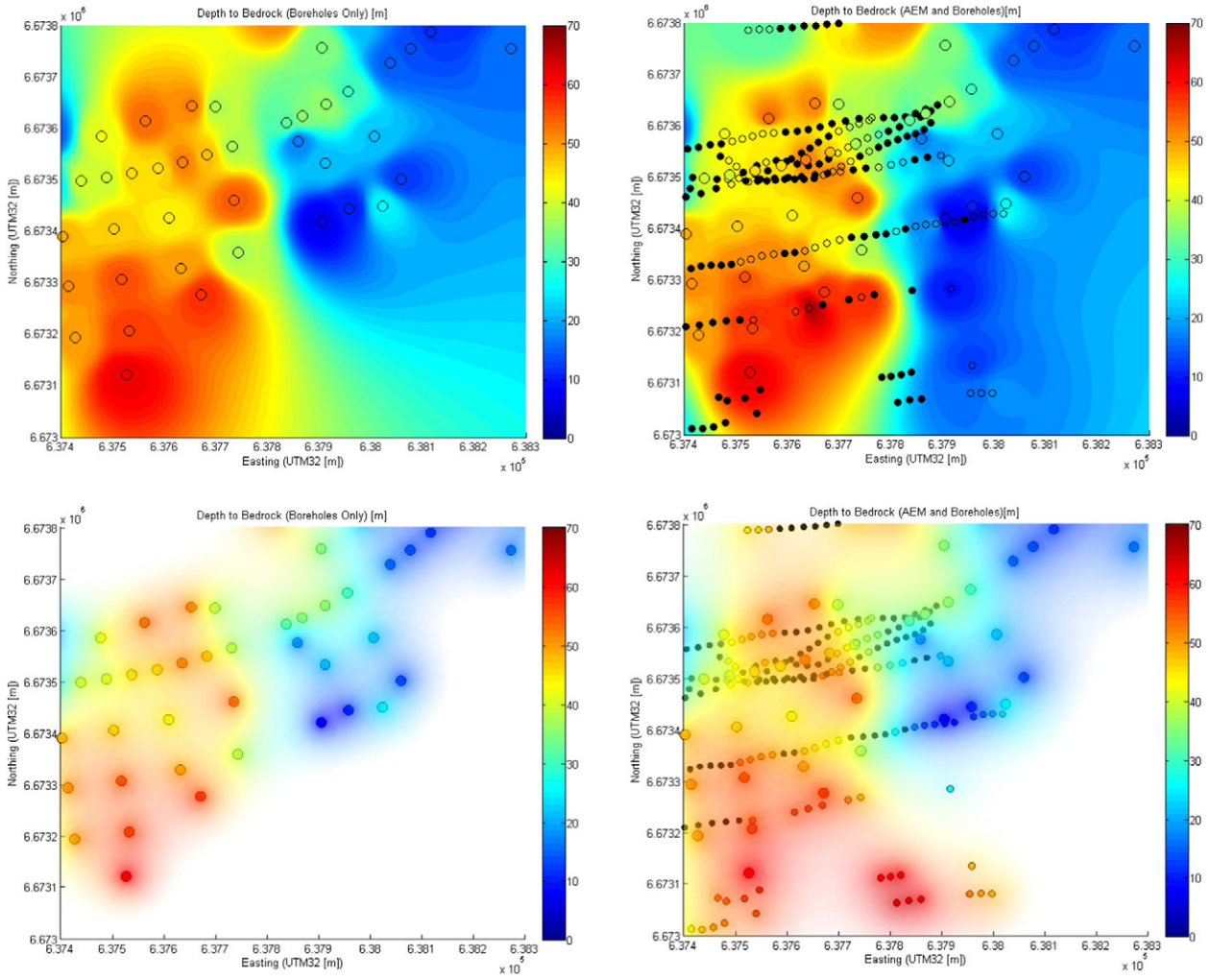

Fig. 8. Comparison of the output depth to bedrock grids using either Variation 1 or 2, and using either only borehole data or including both borehole and AEM data. Small black dots indicated AEM sounding locations where no valid depth to bedrock value was found. The white overlay in Variation 2 represents increasing uncertainty in depth prediction.

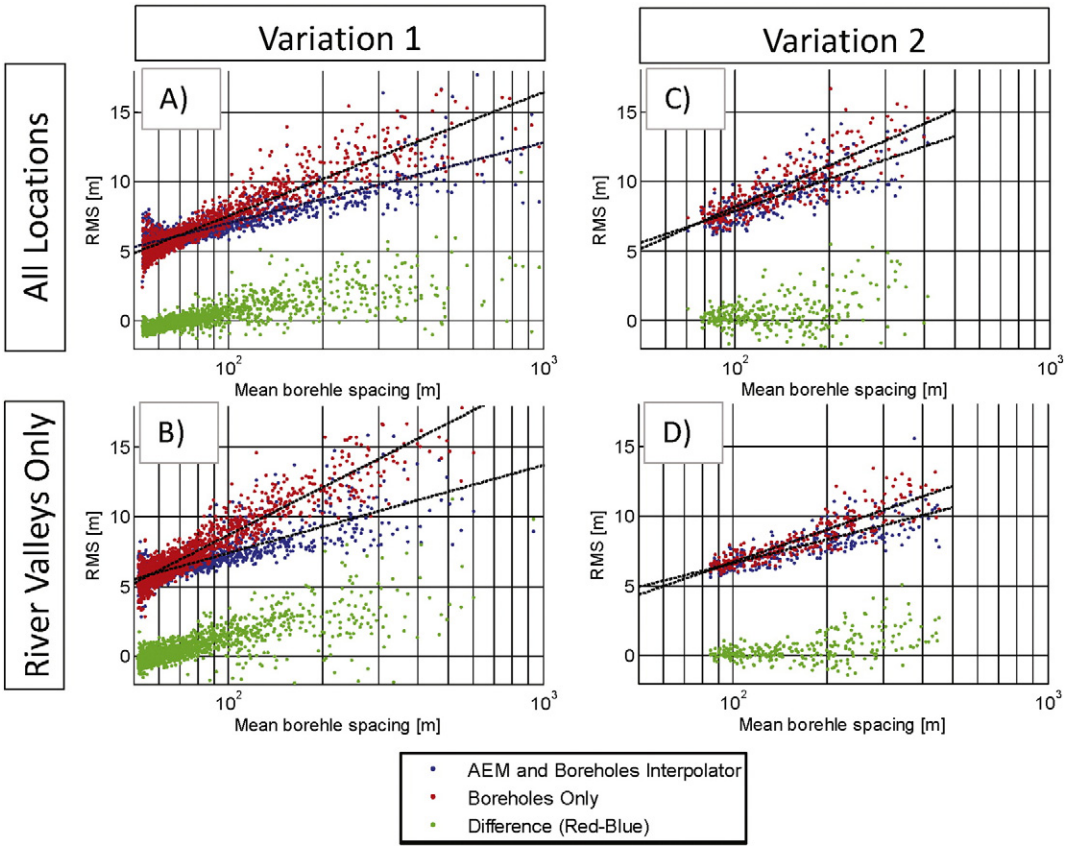

Fig. 9. Results of the cross-validation showing RMS error of the bedrock depth predictions versus mean spacing of the input boreholes. Plots compare accuracy of the models when AEM is used or disregarded, as well as the relative performance of Variations 1 and 2. B) and D) calculate RMS based only on model predictions in river valleys at Uåa and Vorma.

boreholes were rejected as a quality-control measure, leading to additional depth pick rejections in a few isolated instances.

Evaluation of Variation 1 by cross validation shows that using AEM in this way can have a significant comparative advantage over using only boreholes to map depth to bedrock depending on the spatial distribution of boreholes. (Fig. 9A) shows that at large borehole spacings, the average error of the algorithm's depth to bedrock predictions (as expressed in root mean squared (RMS)) tends to be far less than the average error of the borehole only method. This comparative advantage decreases as borehole spacing decreases. The crossover point is at approximately 70 m, roughly half the nominal AEM survey line spacing. Below this point, integrating AEM adds more error to the depth to

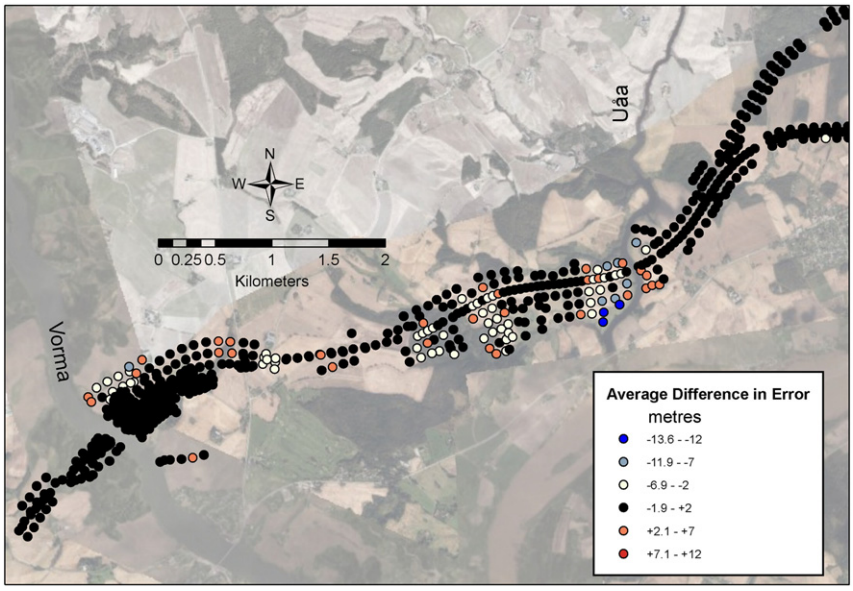

Fig. 10. Cross-validation shows that adding AEM data does not improve the depth to bedrock prediction at most locations (black/approximately zero). However, including AEM data improves the accuracy of the depth to bedrock prediction by up to 13 m in some locations (blue and white/negative). Reductions in accuracy by adding AEM (red/positive) are less frequent and are of a lower magnitude than the improvements.

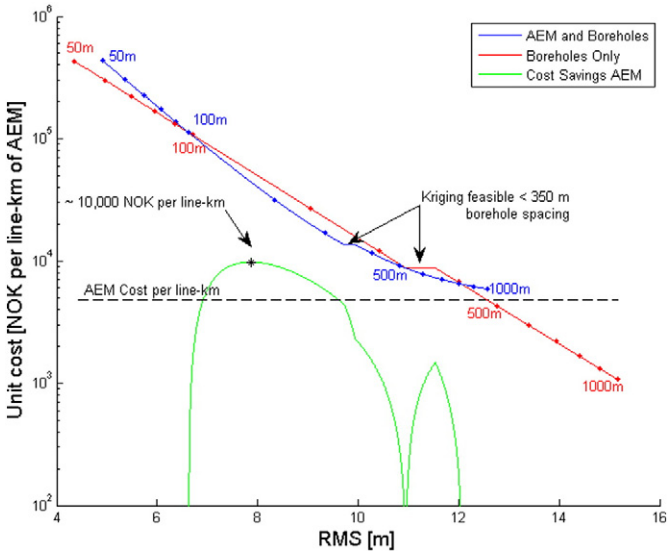

Fig. 11. Unit cost of data collection as a function of target accuracy of the depth to bedrock model. Red and blue labels along the curves indicate the mean borehole spacing associated with the survey. See the Appendix A for derivation of cost models.

bedrock map. A comparison of RMS versus borehole depth showed that the interpolator has more difficulty with outliers, with depth at shallow locations being overestimated, and underestimated at deep bedrock locations. No other significant trends regarding RMS and bedrock depth were found.

Fig. 9A only shows average prediction error and does not account for spatial variation. In most locations, including AEM data does not have a substantial effect on prediction error due to the limited bedrock depth variation in between boreholes. However, in areas with steeper bedrock topography and local maxima and minima, such as the river crossing at Uåa, the comparative advantage of including AEM data versus only using borehole data increases significantly (Fig. 9B).

Evaluation of Variation 2 shows a similar effect (Fig. 9C). When comparing the combined AEM and borehole interpolators between Variations 1 and 2, the second one does appear to have a slight edge in accuracy. The crossover point between Variation 2 and kriging only using borehole depths is also similar, at 90 m mean borehole spacing. However, the average comparative advantage between using both data sets and only boreholes for Variation 1 is much larger than that seen in Variation 2. Nevertheless, the advantage is location dependent too, and produces a modestly better model in locations of difficult terrain (Fig. 10).

Variation 2 does have some weaknesses. Beyond a certain mean borehole spacing, Variation 2 completely fails. When most boreholes are further apart than the average correlation distance (or the *range* in the vocabulary of variogram modeling), a meaningful theoretical semi-variogram cannot be fit because the experimental one derived from the boreholes has no data for small offsets. Furthermore, standard Z-score calculations show that the prediction error estimates should be 1.6 times larger, meaning they are underestimates. No obvious spatial relationship between location and magnitude of underestimate were found. For comparison, calculating z scores for depth predictions using only boreholes and ordinary kriging gives an average score of 1.

5. Discussion

The three stated goals for the depth to bedrock tracking have been met, to varying degrees. Variable bedrock threshold resistivities ranging over more than an order of magnitude were used to select depth to bedrock from resistivity models in two different ways. While Variation 1 lacked uncertainty estimates, those computed by Variation 2 were useful for visualizing the extent of reasonable depth to bedrock predictions, despite being an underestimate. Finally, while some parameter selection is required from the users to select appropriate values for some interpolator parameters, the algorithm offers a large improvement over earlier attempts to extract depth to bedrock from these data sets.

The cross-validation performed indicates that integrating AEM in early phases of geotechnical site investigations in this way can indeed reduce site investigation costs. Fig. 9 shows that when boreholes are sparsely distributed, adding AEM data using this algorithm leads to a substantial enhancement in bedrock model accuracy. This gain in accuracy is much more substantial when data is too sparse for kriging to be possible and simple interpolators from Variation 1 must be used.

However, these figures also show the limitations of using AEM as a detailed bedrock mapping technique. At 125 m line spacing, the survey is already near the lateral resolution limit of the method. It appears that

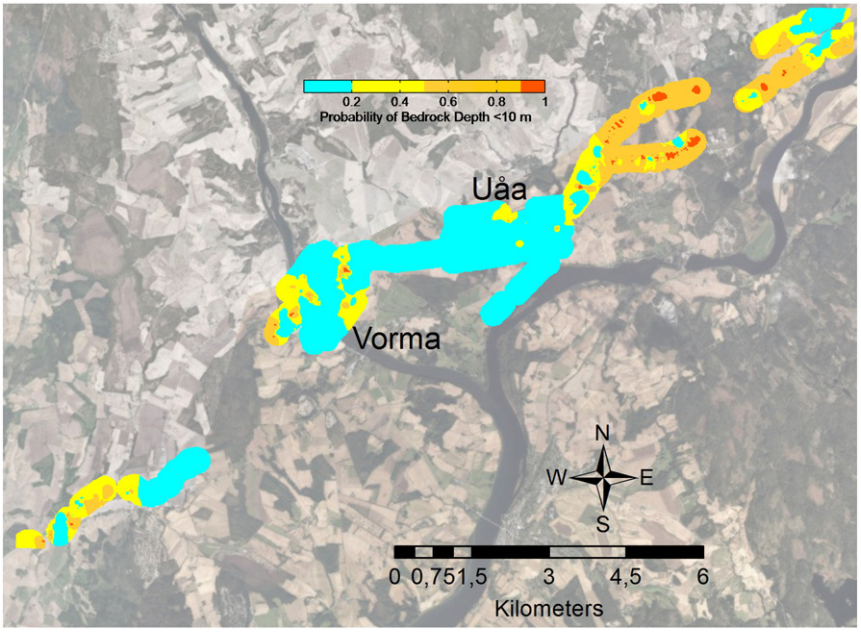

Fig. 12. Probability map of encountering bedrock less than 10 m deep, a potentially useful planning tool for later phases of site investigation.

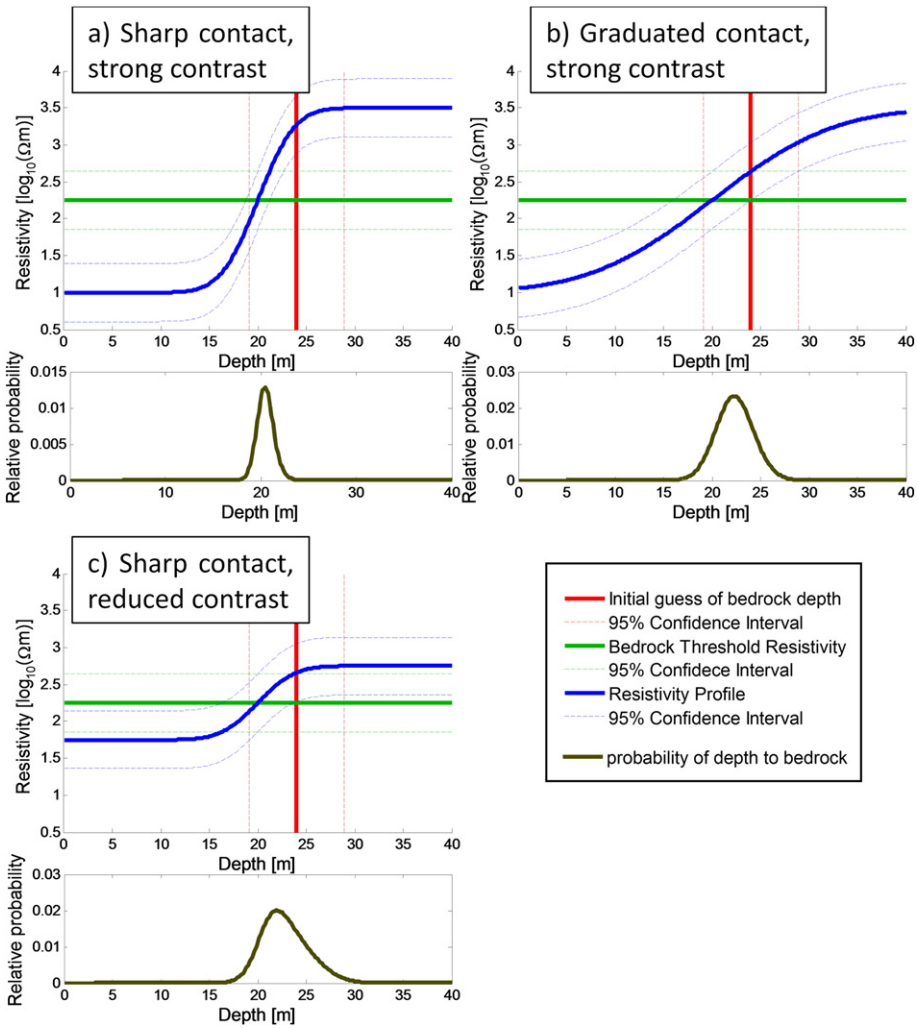

Fig. 13. A comparison of algorithm performance in different, hypothetical geological scenarios. A) a case like the project presented, where there is a sharp boundary between bedrock and overburden resistivity and the difference in resistivity magnitude between domains is large. B) a case where the bedrock-overburden contact has a gradual transition in resistivity. C) A case where the difference in resistivity between overburden and bedrock is not as large.

once borehole spacing becomes much finer than this, the algorithm continues to equally weigh the imprecise depth estimate from the resistivity model and the precise borehole measurements, resulting in an accuracy reduction rather than an improvement. This treatment may not be appropriate because the depth measurements and depth picks based on AEM have very different uncertainties associated with them. Regardless, even if this weakness is addressed, the algorithm performance cannot be expected to outperform a measured data set with a resolution that exceeds that of the geophysical method itself.

Based on estimated unit costs for boreholes and performing an AEM survey and on the average trends in Fig. 9, we have attempted to quantify the cost savings potential that AEM could have provided in this case. Fig. 11 shows unit cost (in Norwegian Kroner per square kilometer) of data acquisition as a function of the target accuracy for the final depth to bedrock model, expressed as the RMS error. Our analysis shows that for early phases of site investigation, combining AEM and borehole data using this algorithm could have provided a comparably accurate bedrock model for 1000 to 10,000 NOK less per line-km of AEM survey (approximately $160 to $1600 USD per line-km) than a ground investigation based on boreholes alone. Details of this calculation are provided in an Appendix A. This is only a first-order estimate given that, among other factors, the uncertainty of the correlation between RMS and mean borehole spacing is not considered. This comparison is also site specific, as the spatial variability of depth and bedrock resistivity play a role in the relative accuracy of each algorithm variation. Furthermore, we have assumed that the cost of collecting AEM data is internal; in some cases, public or third-party datasets (e.g. mineral exploration data) may be used as algorithm input instead. These factors considered, we take the results as evidence that tracking depth to bedrock with this algorithm could have provided large cost savings for early survey results for the E16 highway project, and may be able to do the same for similar engineering projects in the future.

An important caveat is that this preceding cost analysis only considers average trends; actual cost savings provided by AEM may be greater than suggest by Fig. 11. The algorithm using AEM data is not precise enough for detailed bedrock mapping, yet it can still reduce the final number of boreholes used by giving an early indication of where high priority areas are. For instance, while including AEM data only provides minor gains in accuracy in flat areas, it more accurately images locations where bedrock topography varies significantly. Using this, areas without higher spatial variability can be selected for more detailed investigation. The depth uncertainty estimates can also be used to map the probability of encountering bedrock within a certain depth interval

Table 2
Estimated typical unit costs for drilling.

Drilling technique	Cost per 20 m hole (Norwegian Kroner)
Total sounding	10,000
Rotary pressure sounding	8500

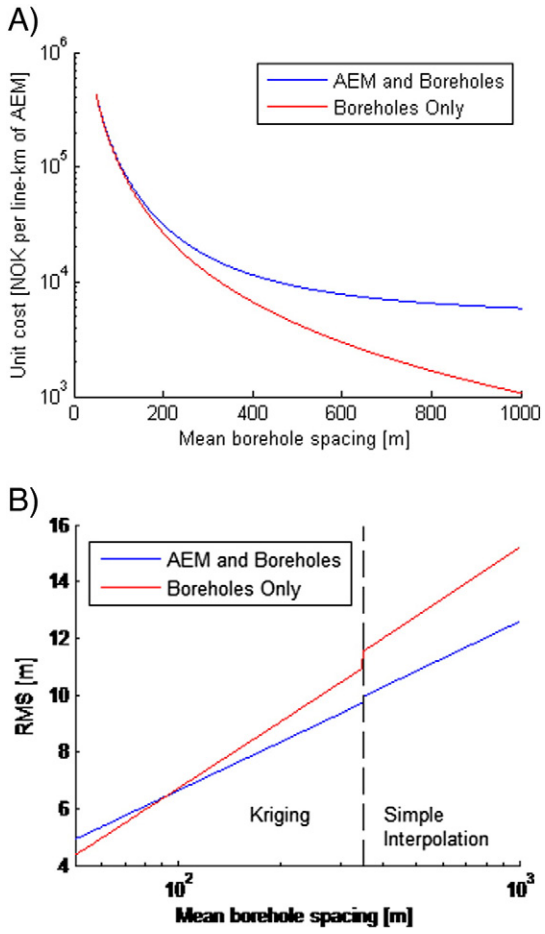

Fig. 14. Plots of two intermediate functions which are combined to model cost as a function of Depth to bedrock prediction accuracy.

(Fig. 12). Moreover, even if kriging is not possible when boreholes are too sparsely sampled, the resulting depth map may be used to estimate the spatial variability of depth, a value which may be used to select an appropriate sample spacing for later stages of the survey. Hence, by carefully considering of the spatial trends observed in an early AEM survey, further reductions in the number of boreholes needed are possible.

The applicability of this method in future projects may also differ because of challenges with this particular AEM data set. With more than 1/3 of AEM data points excluded due to noise, low signal, or inversion model uncertainty, issues with data quality undoubtedly reduced the gains obtained by including AEM data. For parts of the survey a frequency domain system may have been more robust to electric interference and also could have resolved even shallower bedrock depths du to bandwidth difference between frequency- and time domain systems. The primary target of the survey, however, were the areas with tens of meters with conductive clay and high resolution of subtle resistivity variations was important for quick clay delineation. Thus, SkyTEM 302 was the ideal system for this survey. If this algorithm is applied in areas where data quality or challenging inversion situations are not as problematic, we anticipate an improved performance over that demonstrated in this case study.

Table 3
Best fit relationships between RMS of depth predictions and mean borehole spacing (s) given in Fig. 9.

	Variation 1	Variation 2
AEM and Boreholes	$\text{RMS} = 5.771 * \log_{10}(s) - 4.744$	$\text{RMS} = \begin{cases} 5.696 * \log_{10}(s) - 4.766, & \text{for } s<350\text{m} \\ \text{Undefined}, & s>350 \end{cases}$
Boreholes Only	$\text{RMS} = 7.986 * \log_{10}(s) - 8.786$	$\text{RMS} = \begin{cases} 7.805 * \log_{10}(s) - 8.909, & \text{for } s<350\text{m} \\ \text{Undefined}, & s>350 \end{cases}$

Other study areas may present challenges that were not encountered in this project. Some of these could be overcome with slight modifications to the algorithm. The magnitude of resistivity contrast between layers could be smaller (Fig. 13c) where, for example, large shear zones with more conductive minerals or water-filled fractures are present. The existing depth-selection method would assign a very large uncertainty in such a case, but including resistivity gradients as an additional criterion for depth selection could help reduce that uncertainty. When determining the bedrock threshold resistivity at borehole locations in Step 1, it was assumed data points at a similar depth were representative of bedrock resistivity. This may not necessarily be the case where there are larger vertical discontinuities in resistivity, whether due to a geological contact or a fault. When using the same variogram model for interpolation, kriging does not take into account the variability of nearby data points when determining a variance value, but rather only their spatial arrangement. This error could be avoided by including a priori information about geological structures by, for instance, setting linear boundaries across which data points cannot be accessed for interpolation, or by dividing the study area into geological domains where spatial variability is modeled separately. Our method may be more difficult to adapt in other geological conditions. It is common in Canada and Scandinavia for weathered, conductive layers to have been removed by recent glacial erosion, but this is not the case in other areas of the world (Palacky, 1987). A more gradual transition in resistivity would have led to a greater uncertainty in the depth selection (Fig. 13b). Although in Variation 2, Step 3 our algorithm does give more weight to the initial depth estimate based on nearby boreholes when the AEM data is unable to give a precise depth selection, that larger uncertainty is not accounted for when interpolating in Step 4 when creating the final depth map. Thus, while data acquisition and inversion were challenging in our study area, this was an ideal case in terms of strong resistivity contrasts, sharp bedrock-overburden contact, and lack of major, discrete geological structures.

Aside from these modifications to improve the versatility of this tool for other geological settings, there are several changes that would improve overall performance. The highest priority change would be accounting for differences in data point uncertainty when interpolating. This applies primarily to Step 4, where precise borehole measurements and imprecise resistivity model depth picks are combined to create a depth map. A more probabilistic approach would improve the performance of the interpolator in cases where borehole spacing is approaching (but is still more sparse than) the lateral resolution of AEM. Second, the reason why the uncertainty estimates calculated by Variation 2 are underestimates remains unclear. The variogram modeling and kriging gives appropriate variance estimates when excluding AEM data using only borehole information. Hence, the underestimate is likely due either to uncertainty values in the inversion model being too low or due the PDFs being combined in an inappropriate way in Step 3. Incorporating sensitivity values as well as uncertainties from the inversion output may also help address this. Finally, aside from providing uncertainty estimates, using kriging in Variation 2 provided only small accuracy advantages over Variation 1. The ordinary kriging approached did not use existing trends in the data or account for changes in spatial variability over the 30 km long survey extent. More advanced methods such as using Bayesian kriging, accounting for directional anisotropy, or using location-dependent variogram models rather than an area-wide model may warrant investigation (Boisvert, 2010; Omre and Halvorsen, 1989).

6. Conclusion

We have successfully created a depth to bedrock tracking algorithm which combines AEM and borehole data and can account for variable bedrock resistivity. We can quantify prediction error given sufficient borehole information, yet these are underestimates. Finally, while some user input is required to find reasonable bounds on interpolation parameters, the algorithm is far more efficient than the cognitive modeling approach previously used in this project.

Evaluation of the algorithm developed shows that the cost of site investigations can be significantly reduced by using this method. Based on our cross-validation of the algorithm, combining AEM and borehole data in this way can reduce costs for this type of site investigation by 1000 to 10,000 NOK/km depending on the desired accuracy of the depth to bedrock model. The tool is only applicable to early phases of site investigation, however, due to the precision limits of the geophysical measurements themselves.

Despite the measurement resolution limitations, by using AEM this algorithm in an early phase of site investigation, we can (a) identify zones where shallow bedrock is likely to be; (b) identify areas of steep or locally anomalous of bedrock topography; and (c) estimate the spatial variability of depth, giving a more informed choice of borehole spacing. Acquiring a detailed depth to bedrock model should typically be more cost efficient by using AEM because secondary phases of drilling can be planned to target high-priority areas. The degree to which this is feasible is likely very site-dependent. The potential benefits of using the algorithm were limited by issues with data noise from ground infrastructure, low signal, and large uncertainties in the inverted resistivity model. However, the contrast between overburden and bedrock resistivity was strong in our example. We suspect that with some modifications, our method may be applied to cases where geological conditions are not ideal for mapping the bedrock-sediment interface, but further testing is required.

Acknowledgments

We thank the Norwegian Public Road Authority (SVV), in particular road design manager Arvid Sagbakken, for financing this study and giving permission to publish.

In the presented case study NGI acted as a geotechnical advisor to COWI and we are grateful to Frode G Bjørvik for supporting our concept to use a combined geophysics and geotechnical approach. Numerous colleagues at NGI have contributed to our results presented here, Steinar Herman, Kristoffer Kåsin, Kristine Ekseth and Magnus Rømoen to name a few. Thank you especially to Asgeir Kydland Lysdahl for preparing location and sedimentary maps for us (Figs. 1 and 3).

We also thank Dr. Alexander Braun for supervising a portion of this work undertaken at Queen's University, Kingston, ON, Canada.

Neither SkyTEM Surveys nor Århus University have directly contributed to this work but we would not have gotten to these results without SkyTEM's focus on innovative systems and excellent data acquisition and a general collaboration between NGI and the hydrogeophysics group at Århus University.

Appendix A. Cost Estimate Calculations

The cost of data collection per line km of AEM data was the combined total of borehole and AEM data costs:

$$\frac{\text{data collection cost}}{\text{line km}} = \frac{\text{borehole cost}}{\text{line km}} + \frac{\text{AEM cost}}{\text{line km}}.$$

Estimating a unit cost for the AEM survey is non-trivial as factors such as survey size, survey location, season and the system/contractor selection play a significant role in the pricing of the survey. The costs for the AEM survey in the project presented were comparably high for a number of reasons. Potential final project cost savings may thus be considered a minimum estimate. The AEM cost estimate is based on 860,000 NOK for a project of this size, based on 178 survey line km (not including processing and inversion). This gives a value of approximately 4,830 NOK per line km.

The unit cost of boreholes is given by:

$$\frac{\textit{borehole cost}}{\textit{line km}} = \frac{\textit{cost}}{\textit{borehole}} \times \frac{\textit{borehole}}{\textit{area}} \times \frac{\textit{area}}{\textit{line km}}$$

The cost per borehole was estimated using typical costs for geotechnical and geophysical work during the 2014 project (Table 2). In this particular project, roughly 92% of boreholes were rotary pressure soundings and 8% were total soundings. Hence, the weighted mean cost of boreholes for further calculations was 8,620 NOK per 20 m hole.

For most of the survey area, boreholes were arranged on a nominally rectangular grid. Hence, for a given spacing s, the density of boreholes per unit area was:

$$\frac{\textit{borehole}}{\textit{area}} = \frac{1\ \textit{hole}}{s^2\ \textit{km}^2}$$

The footprint of a typical AEM line was estimated to be 125 m wide. Combining these assumptions together, the unit cost of borehole data as a function of mean borehole spacing is:

$$\frac{\textit{borehole cost}}{\textit{line km}} = \left(10260\frac{\textit{NOK}}{\textit{hole}}\right) \times \left(\frac{1\ \textit{hole}}{s^2\ \textit{km}^2}\right) \times \frac{(0.125\ \textit{km} \times 1\textit{km})}{\textit{line km}}$$

$$\frac{\textit{borehole cost}}{\textit{line km}} = \frac{1282.5}{s^2}\frac{\textit{NOK}}{\textit{line km}}$$

Unit cost of data collection as a function of borehole spacing is given in Fig. 14A.

The RMS error of a bedrock depth model was modeled as a function depth of borehole spacing (Table 3) using the results of the algorithm cross evaluation shown in Fig. 9.

Two piecewise functions were constructed: one for the AEM and Boreholes algorithm, and one for the boreholes only interpolation. For a given borehole spacing, the functions returns either the RMS of the model calculated by either Variation 1 or Variation 2, selecting whichever value was smaller (Fig. 14B).

The final cost analysis Fig. 11 was constructed by plotting borehole spacing, data collection cost, and RMS in three dimensions, and then looking at the desired 2D section.

References

Andersen, B.G., 1979. The deglaciation of Norway 15,000–10,000 B. P. Boreas. pp. 79–87.

Anschütz, A., Christensen, C., Pfaffhuber, A.A., 2014. Quantitative Depth to Bedrock Extraction from AEM Data. 20th European Meeting of Environmental and Engineering Geophysics, Athens, Greece, Tu Olym 01 http://dx.doi.org/10.3997/2214-4609.20141994.

Beamish, D., 2013. The bedrock electrical conductivity map of the UK. J. Appl. Geophys. 96, 87–97.

Boisvert, J., 2010. Geostatistics with Locally Varying Anisotropy. PhD Thesis. University of Alberta.

Chilès, J.P., Delfiner, P., 2011. Geostatistics: Modeling Spatial Uncertainty. second ed. Wiley, New York.

Chouteau, M., Boudour, Z., Parent, M., Marcotte, D., 2013. Estimation of overburden thickness using airborne time-domain EM data and a few drill hole data. 13th SAGA Biennial Conference and Exhibition, Mpumalanga, South Africa. South African Geophysical Association.

Foged, N., 2014. Integration of borehole and airborne transient electromagnetic data for automatic compilation of large scale hydrogeological models. PhD Thesis. Aarhus University.

Foged, N., Marker, P.A., Christansen, A.V., Bauer-Gottwein, P., Jørgensen, F., Høyer, A.-S., Auken, E., 2014. Large scale 3-D modeling by integration of resistivity models and borehole data through inversion. Hydrol. Earth Syst. Sci. 11, 1461–1492.

Gunnink, J.L., Bosch, J.H.A., Siemon, B., Roth, B., Auken, E., 2012. Combining ground-based and airborne EM through Artificial Neural Networks for modelling glacial till under saline groundwater conditions. Hydrol. Earth Syst. Sci. 16, 3061–3074.

He, X., Koch, J., Sonnenborg, T.O., Jørgensen, F., Schamper, C., Refsgaard, J.C., 2014. Uncertainties in constructing stochastic geological models using transition probability geostatistics and transient AEM 65 data. Water Resour. Res. 50, 3147–3169.

Jørgensen, F., Møller, R.R., Nebel, L., Jensen, N., Christiansen, A.V., Sandersen, P., 2013. A method for cognitive 3D geological voxel modelling of AEM data. Bull. Eng. Geol. Environ. 72, 421–432.

Michaels, P., 1999. Use of engineering geophysics in the design of highway passing lanes. Proc. of the Symposium on the Appl. of Geophys. to Eng. and Environ. Problems, SAGEEP99, pp. 179–187.
Michaels, P., 2004. Design of geophysical surveys in transportation. Geotech. Eng. for Transp. Proj. 2, pp. 1832–1839
Ngan-Tillard, D., Venmans, A., Slob, E., Mulder, A., 2010. Total engineering geology approach applied to motorway construction and widening in the Netherlands: Part II: Pilot site in tidal deposits. Eng. Geol. 114 (3–4), 171–180.
Nichol, D., Reynolds, J.M., 1999. Ground penetrating radar survey to detect scour holes beneath the A525 highway at Nant-y-Garth Pass, Wales: a case history. Q. J. Eng. Geol. 32, 157–162.
Norwegian Geological Survey (Norges Geologiske Undersøkelse) Kartkatalog. (online), http://geo.ngu.no/kart/kartkatalog/ (Accessed April 11, 2014).
Okazaki, K., Mogi, T., Utsugi, M., Ito, Y., Kunishima, H., Yamazaki, T., Takahashi, Y., Hashimoto, T., Ymamaya, Y., Ito, H., Kaieda, H., Tsukuda, K., Yuuki, Y., Jomori, A., 2011. Airborne electromagnetic and magnetic surveys for long tunnel construction design. Phys. Chem. Earth 36, 1237–1246.
Omre, H., Halvorsen, K.B., 1989. The Bayesian bridge between simple and universal kriging. Math. Geol. 21 (7), 767–786.
Palacky, G.J., 1987. Resistivity characteristics of geologic targets. In: Nabighian, M.N. (Ed.), Electromagnetic Methods in Applied Geophysics Theory vol. 1. Society of Exploration Geophysicists, Tulsa, Oklahoma, USA, pp. 53–129.
Pfaffhuber, A.A., Grimstad, E., Domaas, U., Auken, E., Foged, N., Halkjaer, M., 2010. Airborne EM mapping of rockslides and tunneling hazards. Lead. Edge 29 (8), 956–959.
Pryet, A., Ramm, J., Chilès, J.P., Auken, E., Deffontaines, B., Violette, S., 2011. 3D resistivity gridding of large AEM datasets: A step towards enhanced geological interpretation. J. Appl. Geophys. 75, 277–283.
Ramberg, I.B., Bryhni, I., Nøttvedt, A., Rangnes, K., 2008. The Making of a Land: Geology of Norway. 2008 ed. Norsk Geologisk Forening, Trondheim, Norway.
Rømoen, M., Pfaffhuber, A.A., Karlsrud, K., Helle, T.E., 2010. The use of a CPTU-probe with resistivity module on marine sediments. CPT'10: 2nd international symposium on Cone Penetration Testing Huntington Beach, California.
Rucker, M.L., 2000. Estimating earthwork factors for roadcuts using surface geophysics. Pac. Rocks 2000: Rock Around the Rim: Proc. of the Fourth N. Am. Rock Mech. Symp., pp. 709–714
Sauvin, G., Lecomte, I., Bazin, S., L'Heureux, J.S., Vanneste, M., 2013. Geophysical Data Integration for Quick-Clay Mapping: The Hvittingfoss Case Study, Norway. Adv. Nat. Technol. Hazards Res. 36, 229–239.
Schwanghart, W., 2010. Matlab File Exchange: variogramfit. (online), http://www.mathworks.com/matlabcentral/fileexchange/25948-variogramfit (Accessed 8 September 2014).
Solberg, I.L., Hansen, L., Rønning, J.S., Haugen, E.D., Dalsegg, E., Tønnensen, J.F., 2012. Combined geophysical and geotechnical approach to ground investigations and hazard zonation of a quick clay area, mid Norway. Bull. Eng. Geol. Environ. 71, 119–133.
Sørensen, K.I., Auken, E., 2004. SkyTEM — A new high-resolution helicopter transient electromagnetic system. Explor. Geophys. 35, 191–199.
Starmer, I.C., 1996. Oblique Terrane Assembly in the Late Paleoproterozoic during the Labradorian–Gothian Orogeny in Southern Scandinavia. J. Geol. 104, 341–350.
Strebelle, S., 2002. Conditional simulation of complex geological structures using multiple-point statistics. Math. Geol. 34 (1), 1–21.
Viezzoli, A., Christiansen, A.V., Auken, E., Sørensen, K., 2008. Quasi-3D modeling of airborne TEM data by spatially constrained inversion. Geophysics 65 (2), F105–F113.